Available online at www.sciencedirect.com
SCIENCE DIRECT®
Surface Science 558 (2004) 35–48
SURFACE SCIENCE
www.elsevier.com/locate/susc

Metastable surface structures of the bimetallic Sn/Pt(1 0 0) system

Matthias Batzill [a,*], David Beck [b], Bruce E. Koel [b,*]

[a] Department of Physics, Tulane University, 6400 Freret Street, Stern Hall 2001, New Orleans, LA 70118, USA
[b] Department of Chemistry, University of Southern California, Los Angeles, CA 90089-0482, USA

Received 6 January 2004; accepted for publication 8 April 2004
Available online 22 April 2004

Abstract

An ordered Sn overlayer on Pt(1 0 0) and several metastable Sn/Pt(1 0 0) surface alloys were studied using scanning tunneling microscopy (STM), low energy electron diffraction (LEED), and Auger electron spectroscopy (AES). These surfaces were studied previously using alkali-ion scattering spectroscopy (ALISS), LEED, and CO chemisorption, in order to determine conditions for alloy formation [Surf. Sci. 330 (1995) 193]. In those earlier studies, structural transitions with increasing annealing temperatures from a c(2×2)-Sn overlayer to a c(2×2)-Sn/Pt(1 0 0) surface alloy and finally to a $(3\sqrt{2} \times \sqrt{2})$R45° alloy structure were observed. Here STM is used to determine surface morphologies and atomic scale structures of these alloys. Sn (0.67 ML) deposited on the reconstructed Pt(1 0 0)-hex surface and annealed to 550 K formed a c(2×2)-Sn overlayer with compact, monolayer-high islands with step edges oriented along the [1 0 0] and [0 1 0] azimuths. Annealing the sample to 750 K initiated alloying and a c(2×2) surface alloy formed locally. However, the c(2×2) alloy structure does not appear to be stable even at this early stage of alloying and narrow channels along the ⟨1 0 0⟩ crystallographic directions form. For higher annealing temperatures, these channels evolve to form a two-domain structure with almost equidistant channels along the [1 0 0] and [0 1 0] directions, respectively. A dominant channel separation of $3\sqrt{2}$ times the surface-lattice constant of Pt(1 0 0) is observed. This channel separation gives rise to a streaky $(3\sqrt{2} \times \sqrt{2})$R45° LEED pattern. The channels are characterized by three missing atomic rows. Between these channels are narrow terraces that are predominantly three-atomic-rows wide. The step edges of these terraces are Pt-terminated, while Sn is alloyed in the center of these terraces. A local p(2×2) ordering of alloyed Sn is often observed for wider terraces. Annealing to 1000 K results in "fragmentation" of the narrow terraces to form small, often square, islands with side-lengths as small as $\sqrt{2}$ times the surface-lattice constant of Pt(1 0 0). The structural characterization of these Sn/Pt(1 0 0) surfaces is used to interpret previous chemical adsorption studies.

Keywords: Auger electron spectroscopy; Low energy electron diffraction (LEED); Low energy ion scattering (LEIS); Scanning tunneling microscopy; Catalysis; Surface chemical reaction; Surface stress; Surface structure, morphology, roughness, and topography; Platinum; Tin; Alloys; Low index single crystal surfaces; Metallic surfaces

1. Introduction

Bimetallic alloys comprise an important class of materials that are used extensively for their

* Corresponding authors. Tel.: +1-504-865-5520; fax: +1-504-862-8702 (M. Batzill), Tel.: +1-213-740-4126; fax: +1-213-740-3972 (B.E. Koel).
E-mail addresses: mbatzill@tulane.edu (M. Batzill), koel@usc.edu (B.E. Koel).

0039-6028/$ - see front matter © 2004 Published by Elsevier B.V.
doi:10.1016/j.susc.2004.04.007

physical, chemical, and catalytic properties. Developing additional correlations of surface structure and composition of these bimetallic systems with their chemical and catalytic properties is a key goal of surface science research on these materials. In such investigations, systems are sought that can be prepared with various, well-defined, (meta-)stable surface structures.

The surface composition and structure of a bimetallic system in thermodynamic equilibrium is given by minimization of the surface free energy of the system. Conceptually, one can separate the surface free energy into several components. So, because the cleavage energy can vary for different elements, the surface free energy of a bimetallic surface can be reduced by terminating the surface with the lower cleavage-energy element. And, this may drive segregation of this element to the surface in a bimetallic alloy. Opposing this trend of surface segregation is the exchange energy between elements. The exchange energy in most alloys is negative, i.e., hetero-neighbors are preferred over atomic neighbors of the same element. This favors mixing and consequently often prevents formation of a fully segregated surface layer. Furthermore, surface strain will influence the composition and structure of surfaces. Free surfaces are often under tensile strain that may cause surface reconstruction with a denser atom-packing than corresponding bulk planes. This is observed for instance for pure Pt(1 0 0) surfaces which form a quasi-hexagonal surface layer that is ~22% more densely packed than bulk Pt(1 0 0) planes [1,2]. Strain-relieving surface reconstructions on bimetallic alloys have also been observed for the (1 0 0) faces of $Pt_{10}Ni_{90}$, $Pt_{25}Ni_{75}$, and $Pt_{25}Co_{75}$ systems [3,4]. In addition to surface reconstructions, bimetallic alloys can also reduce tensile or compressive surface strain by segregating the larger or smaller element of the alloy, respectively, to the surface [5]. Conversely, surface segregation driven by cleavage-energy considerations may increase the surface strain due to changes of the lattice constant induced by compositional changes of the surface layer.

While the thermodynamic equilibrium structure for a system is defined by the constellation with the lowest free energy, there always exist kinetic barriers that may prevent the system from obtaining this low-energy structure. These kinetic barriers allow the formation of metastable surface structures.

Bimetallic Pt catalysts, and in some cases (perhaps yet in some undiscovered systems), Pt alloys are of interest because of their many important applications in catalysis. In particular, Sn–Pt alloys are used in hydrocarbon reforming processes and in methanol-oxidation based fuel cells [6,7]. Surface science studies of the Sn–Pt alloy system are reviewed by Speller and Bardi [8]. The surface structure of an ordered Pt_3Sn(1 0 0) bulk alloy under clean, UHV conditions has been characterized [9]. At thermodynamic equilibrium, the surface structure is a simple truncation of the bulk lattice, with c(2×2) ordering, 50% Sn in the surface layer, and a pure-Pt second (subsurface) layer. This indicates that the surface free energy of the alloy is lowered by maximizing the amount of Sn at the surface while maintaining the ordered bulk structure. The latter maximizes the number of Sn–Pt bonds. Altering the preparation conditions of the sample can result, however, in a variety of metastable structures and compositions due to preferential sputtering of Sn and segregation effects during annealing. Ar^+-ion sputtering and low-temperature (600 K) annealing form large pyramidal structures on the surface with primarily (1 0 2) facets on the sides and a 'beaded Pt-row' structure on top and between the pyramids.

Several studies have been carried out to characterize the surface structure of Pt_3Sn(1 1 1) bulk alloys, using low energy ion scattering spectroscopy (LEISS), low energy electron diffraction (LEED), Auger electron spectroscopy (AES), and scanning tunneling microscopy (STM) [10–12]. These investigators have determined that the (1 1 1) face of the alloy primarily has the composition expected from termination of the bulk lattice (Pt_3Sn), however, a Pt_2Sn surface can be formed under conditions of subsurface-Sn depletion [12].

Surface alloys, formed by depositing one element on another and annealing, are an important subset of bimetallic alloys that possess unique characteristics. The term "surface alloy" denotes the presence of an intermixed layer or alloy in the topmost, surface layer only, while the bulk is

mainly composed of a single element. The main difference between surface alloys compared to bulk alloy surfaces is that the bulk lattice constants are different and thus the surface strain due to lattice mismatch between the surface layer and the bulk is different, and this may result in different structures. Generally, the strain is larger in surface alloys then in bulk alloy surfaces.

Our group has taken the approach of forming surface alloys to study effects of surface composition and structure on the chemistry of Sn–Pt alloys. By depositing Sn films on Pt(1 1 1) or (1 0 0) single crystals and annealing, several different, ordered *surface alloys* can often be prepared depending on the initial coverage and annealing temperature. For example, an ordered (2×2) or $(\sqrt{3}\times\sqrt{3})$R30° surface alloy can be prepared on a Pt(1 1 1) single crystal surface depending on the amount of Sn deposited [13]. The formation of these ordered surface alloys can be understood by the energy considerations discussed above. The Sn–Pt system strongly favors Pt–Sn bonds over Sn–Sn bonds and this always results in Sn atoms surrounded by Pt atoms. The lower cleavage energy of Sn compared to Pt provides a driving force for Sn to remain at the surface. Additionally, the larger atomic size of Sn compared to that of Pt causes strain in the Pt-host lattice upon alloying. This strain can be more easily reduced at the surface than it could be in the bulk, and consistently, it has been observed that Sn atoms are buckled outward from the surface plane as a response of this surface strain [14].

While the surface structures of Sn–Pt(1 1 1) surface alloys are characterized well, there remain open questions about the surface structures formed upon deposition of Sn and alloying on the Pt(1 0 0) surface. In this communication the structures of such Sn–Pt(1 0 0) surfaces are investigated. Previous studies by LEED and ALISS showed that depositing 1 monolayer of Sn on Pt(1 0 0) and annealing to 550, 750, or 900 K results in the formation of a $c(2\times2)$ overlayer, $c(2\times2)$ surface alloy, and $(3\sqrt{2}\times\sqrt{2})$R45° surface alloy, respectively [15,16]. (Throughout the remainder of this text, we will often use a shorthand notation and denote this latter alloy as the $3\sqrt{2}$ alloy.) Here, STM is added as a structural characterization tool. This new insight allows us to present a structural model for the $(3\sqrt{2}\times\sqrt{2})$R45° surface alloy. This structural characterization is particularly important for establishing new structure–reactivity correlations.

In previous studies, chemisorption of CO [17], NO [18], and C_2D_2 [19,20] on Sn/Pt(1 0 0) surface alloys has been investigated. Alloying reduced the saturation coverage of CO from 0.77 ML on a clean Pt(1 0 0) substrate to 0.28 ML on the $c(2\times2)$ alloy and 0.25 ML on the $3\sqrt{2}$ alloy. NO coverages in the monolayer followed this trend as well, but additionally the reaction pathway was altered from that on clean Pt(1 0 0) to favor N_2O production on the alloy. A similar trend in the saturation coverage of C_2D_2 was observed upon alloying and again a change in the reaction chemistry at the alloy surface was seen. In this case, benzene was produced via acetylene cyclotrimerization *on the* $3\sqrt{2}$ *alloy only* and not on the $c(2\times2)$ alloy nor clean Pt(1 0 0) surfaces. This result suggests an important structural difference between the alloy surfaces that was not revealed in prior characterizations of these surface alloys.

2. Experimental methods

All experiments described in this report were performed in an ultra-high vacuum (UHV) chamber with a base pressure of 2×10^{-10} Torr [21]. The apparatus was equipped with reverse-view LEED-optics, cylindrical mirror analyzer (CMA) for AES, quadrupole mass spectrometer (QMS) for residual gas analysis, ion sputtering gun for sample cleaning, leak valves and gas dosing lines, and resistively heated Sn doser made using a Ta-boat. The STM was a home-built, single piezo-tube design. Electrochemically etched polycrystalline-tungsten tips were used in all experiments. STM images were obtained in the constant-current mode exclusively with the bias voltage applied to the tip.

Standard procedures for cleaning the Pt single crystal and preparing the Sn/Pt(1 0 0) surface alloys were used [15,16]. The Pt(1 0 0) single crystal was cleaned using cycles of 500-eV Ar^+-ion sputtering followed by annealing at 1000 K in 2×10^{-7}-Torr

O_2. Once clean, the sample was annealed at 1200 K for 30 s to form the Pt(1 0 0)-hex-R0.7° reconstructed surface [22,23]. The cleanliness of the sample was checked using AES and the surface ordering was confirmed using LEED.

Sn coverages were determined by comparison to a Sn-AES uptake plot performed for a Pt(1 1 1) single crystal under otherwise identical conditions. The "break" in this curve for completion of the Sn monolayer gave a Sn(430 eV)/Pt(237 eV) AES ratio of 8.2 which corresponds to a Sn coverage of 1.47×10^{15} cm^{-2} for a hexagonal close-packed Sn structure. The Sn flux was estimated to be 0.013 ML/s, and a constant value of the flux was used for all experiments.

A description of the preparation of these ordered Sn/Pt(1 0 0) surfaces has been given by Li and Koel [15]. In the studies reported here, Sn was deposited on the Pt(1 0 0)-hex surface at 330–380 K. A Sn coverage of 0.67 ML was deposited to form the c(2×2)-Sn overlayer and a Sn coverage of 1.1 ML was used to form the two alloys. Following Sn deposition, the sample was annealed to 550, 750, or 900 K in order to form the desired c(2×2) overlayer, c(2×2) alloy, or $3\sqrt{2}$ alloy, respectively. The annealing time was 30 s in all cases. Sn coverages, Θ_{Sn}, in this paper are referenced to the unreconstructed, (1×1)-Pt(1 0 0) surface atom density, so that $\Theta_{Sn} = 1$ ML corresponds to 1.3×10^{15} cm^{-2}.

3. Results

The clean Pt(1 0 0) surface reconstructs to form a hexagonal overlayer. STM images (not shown) exhibit the characteristic features of the hexagonal reconstruction [24]. The LEED pattern of the hex-reconstructed surface is shown in Fig. 1a. This was the initial state of the Pt(1 0 0) surface for all subsequent experiments.

3.1. c(2 × 2)-Sn overlayer on Pt(1 0 0)

AES spectra collected after Sn-deposition at room temperature and after subsequent annealing of the sample to 550 K showed a Sn(430)/Pt(237) ratio of 4.6 and 4.3, respectively. This only slight reduction in the Sn/Pt ratio excludes Sn diffusion into the bulk as an important process at these temperatures, but does not distinguish between overlayer and incorporated alloy formation. Previous ALISS and CO-chemisorption studies established that this preparation procedure forms a c(2×2) ordered Sn overlayer. A LEED pattern with slightly diffuse c(2×2) spots and sharp primary spots was observed for this surface and is shown in Fig. 1b. The LEED pattern shows that the Pt-hex reconstruction has been lifted. Diffuse c(2×2) spots suggest relatively small domains. The high background intensity indicates appreciable disorder in the structure.

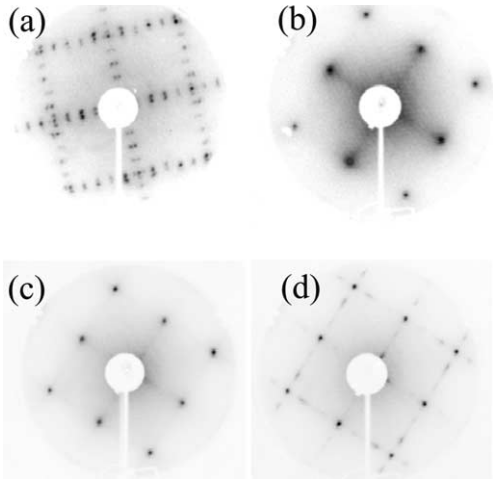

Fig. 1. LEED pattern of (a) Pt(1 0 0)-hex reconstruction taken at an electron energy of 65 eV, (b) Pt(1 0 0) with a Sn-c(2×2) overlayer (56 eV), (c) SnPt(1 0 0)-c(2×2) surface alloy (57 eV), (d) SnPt(1 0 0)-$3\sqrt{2}$ surface alloy (62 eV).

An STM image of the Sn-overlayer surface is shown in Fig. 2. The square lattice of the unreconstructed (1 0 0) substrate exerts a strong influence on the annealed overlayer, forming compact island structures with edges oriented predominately along [1 0 0] and [0 1 0] directions. These are the densely packed directions for a c(2×2) overlayer. The formation of step edges with preferential crystallographic orientations indicates that there is either a strong interaction between the atoms in the overlayer or that the underlying substrate acts as a template. The formation of an "open" c(2×2) overlayer, with an atom-spacing of

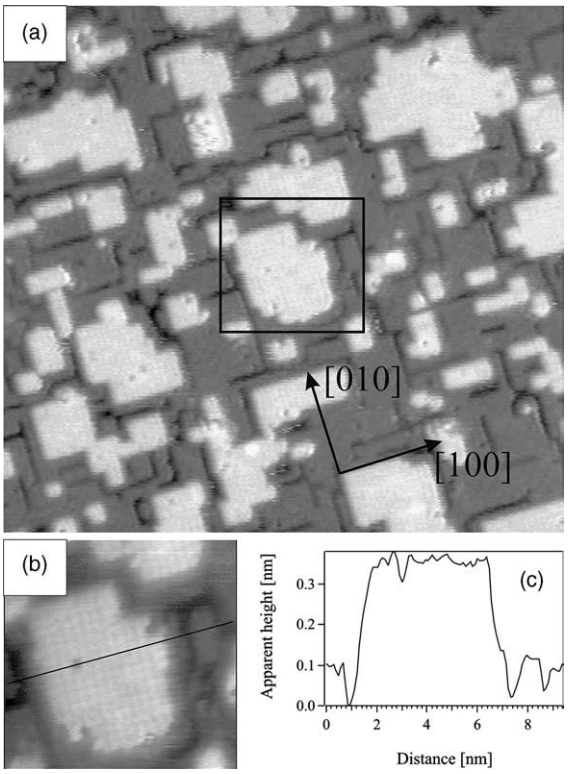

Fig. 2. STM images of a c(2×2)-Sn overlayer. (a) Scan size (50 nm×50 nm). Step edges of the islands are oriented along the ⟨1 0 0⟩ directions. Channels of missing Sn are imaged on the lower terrace. These channels are also aligned along ⟨1 0 0⟩ azimuths. (b) High resolution image of c(2×2) overlayer with an interatomic spacing of 3.9 Å. In the middle of the island a Sn-vacancy is imaged. The line indicates a cross-section that is displayed in (c).

$\sqrt{2}$ times the surface-lattice constant of Pt(1 0 0), rather than a densely packed overlayer, as is frequently observed for metal on metal epitaxial systems in the monolayer regime, is further verification of a relatively weak Sn–Sn interaction compared to the stronger Sn–Pt interactions that force Sn atoms to adsorb in fourfold-hollow sites of the Pt(1 0 0) substrate. Occupation of every fourfold-hollow site by Sn-adatoms and thus formation of a pseudomorphic overlayer is not allowed because of the larger atomic size of Sn compared to Pt (2.81 versus 2.77 Å).

In the STM image shown in Fig. 2a, one can see three different apparent height levels. Islands (white regions) cover 38% of the surface. Intermediate and dark regions (between the islands) account for 50% and 12% of the surface, respectively. The islands display c(2×2) ordering and are one-monolayer high (2.4 Å). Areas between islands exhibit mostly c(2×2) and some p(2×2) ordering. The p(2×2) regions are apparently too small to be observed in LEED. Dark "channels" in the image have an apparent depth of 1.15 ± 0.15 Å.

An island in Fig. 2a identified by the superimposed black square is shown in a separate image in Fig. 2b. In this image, the c(2×2) ordering can be seen clearly. For a Sn-*overlayer*, the position of the Sn adatoms are presumed to be imaged as "bright". Fig. 2c shows a cross-section across the island on top of the brightest features. The image and line scan reveal a point defect which has an apparent depth of 0.7 Å. Such depressions are often observed in the c(2×2)-overlayer islands and these are attributed to missing Sn atoms in the adlayer. An increased density of vacancies in such an open overlayer structure with weak intralayer interactions compared to a densely packed surface layer is expected as a consequence of a decreased formation energy for vacancies in open structures.

The presence of islands on the surface may arise from lifting of the Pt-hex reconstruction upon deposition of Sn. Since the hexagonally close-packed (hex) Pt surface layer accommodates 20–25% more Pt than does the bulk-terminated (1 0 0) surface [1,24], Pt atoms are ejected out of the surface layer when Sn deposition lifts the reconstruction. The Pt atoms expelled into the adlayer then may alloy with deposited Sn adatoms. This mechanism has a lower barrier for alloying than alloying by *interlayer* atom exchange and thus alloying in the adlayer takes place at lower temperatures. Similar mixing of deposited elements with expelled Pt atoms from the hex-reconstruction has been reported previously [25–27]. This mechanism ceases, however, once the reconstruction of the entire surface is removed and a Pt(1 0 0)-1×1 substrate is formed. Subsequent Sn deposition will cover both Sn–Pt alloy islands as well as the areas in between with Sn adatoms. Mild annealing of the surface to 550 K will allow agglomeration of Sn–Pt alloy islands, which

requires only *intralayer* diffusion. This temperature is apparently still too low to activate extensive diffusion and incorporation of Sn adatoms from the overlayer into the Pt substrate to form more extensive Pt–Sn alloy phases.

The fraction of the STM image corresponding to the different regions (white, intermediate, and dark) can be used to interpret these structures. Our best estimate of the initial Sn coverage prior to annealing was 0.67 ML. Islands and intermediate-height regions cover 88% of the area imaged in Fig. 2. These areas are covered by a predominately c(2×2)-Sn overlayer corresponding to a Sn coverage of 0.44 ML. Dark "channels" covering 12% of the surface are tentatively described as areas not covered by Sn. Therefore, a discrepancy of 0.23-ML Sn exists. This amount of Sn could be present in a second-layer (beneath the Sn-adlayer) Sn–Pt alloy formed by expelling the excess 20–25% Pt from the hex-reconstruction. Thus, the "missing" Sn would be combined to form an alloy with a composition close to $Pt_{50}Sn_{50}$, such as that, for example, observed for the c(2×2) alloy discussed in the next subsection. Clear evidence of the presence of Sn in the second layer under these preparation conditions also comes from previously published ALISS data (as discussed below).

3.2. Sn/Pt(1 0 0)-c(2 × 2) surface alloy

Previous studies indicated that a Sn/Pt(1 0 0)-c(2×2) *incorporated surface alloy* can be prepared by depositing 1.1-ML Sn onto a Pt(1 0 0)-hex substrate and then annealing the sample to 750 K. These studies concluded that the overlayer-to-alloy transition occurs within a narrow temperature window of 700–750 K [15]. The excess amount of Sn required to form this surface alloy, which incorporates a maximum amount of 0.5-ML Sn in the topmost surface layer, indicates that Sn diffusion into the bulk of the Pt crystal also takes place at these temperatures. AES spectra collected before and after annealing show a Sn(430)/Pt(237) ratio of 8.2 and 5.6, respectively, i.e., a significant reduction of Sn in the surface layer. This is consistent with alloy formation and diffusion of Sn into the bulk. Not all of the excess Sn is dissolved deeply into the bulk, but a significant amount remains close to the surface in the second layer. This second-layer Sn gives rise to an enhanced scattering peak at 70° in ALISS spectra (as discussed below). A sharp c(2×2) LEED pattern was observed for this surface and the corresponding photograph is shown as in Fig. 1c.

The STM image shown in Fig. 3 reveals that the surface is highly structured with *six levels* observed as different heights. All of these terraces have step edges oriented along the ⟨1 0 0⟩ directions, as was the case for overlayer islands. In the image in Fig. 3a, the surface is covered by two general types of structures. The topmost terraces (with a height of

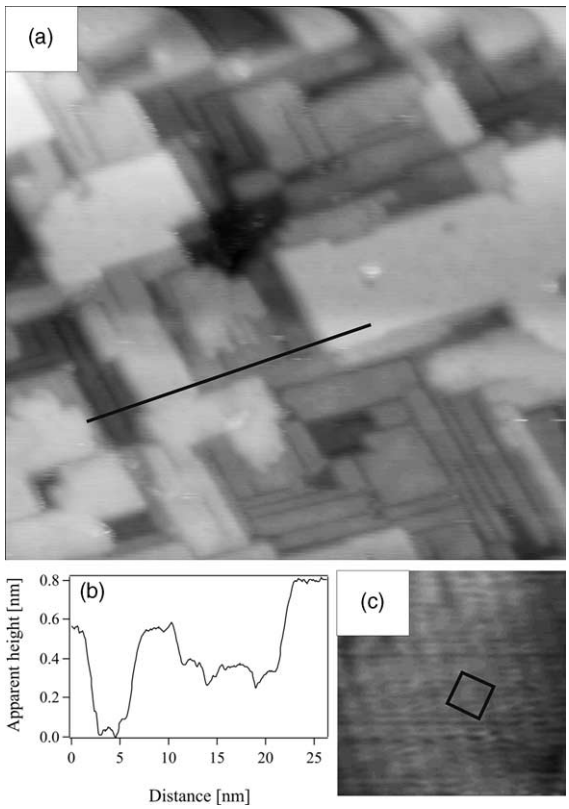

Fig. 3. (a) STM image of a Sn/Pt(1 0 0)-c(2×2) surface alloy. The line indicates a cross-section displayed in (b). The surface exhibits several terraces. Some terraces exhibits channels that are characteristic for a $3\sqrt{2}$ surface alloy structure that forms at slightly higher annealing temperatures. (c) Small-area STM image with a c(2×2) unit cell indicated.

0.8 nm in the line scan in Fig. 3b) are atomically flat and show c(2×2) ordering (Fig. 3c). The other levels are terraces separated by step heights of about 0.2 nm. Lower terraces are intervened by straight channels oriented in the [0 1 0] or [1 0 0] direction. The atomic contrast with a c(2×2) periodicity observed in STM on the top terraces is believed to arise from imaging Pt atoms. An atomic corrugation between protrusions and depressions of 0.1–0.2 Å is observed. The imaging of Pt as protrusions and Sn as depressions in Pt–Sn alloys has been discussed in detail previously [12,28]. The terraces intervened by dark channels illustrate the onset of restructuring of the surface into a $3\sqrt{2}$ alloy that forms extensively upon annealing to slightly higher temperatures. This structure will be characterized in the next subsection.

In these investigations, we never observed a surface that could be characterized as solely due to a c(2×2) alloy phase. Therefore, this is a metastable structure that only exists in small domains. The highly corrugated nature of the surface is a consequence of the intermixing of Sn with bulk Pt during the alloying process. A higher annealing temperature is needed to smoothen the surface, but this would inevitability destroy the metastable c(2×2) alloy structure.

3.3. Sn/Pt(1 0 0)-($3\sqrt{2} \times \sqrt{2}$)R45° surface alloy

A third, ordered alloy structure was prepared by depositing 1.1-ML Sn on the Pt(1 0 0)-hex surface and then annealing to 900 K [15,16]. After this procedure, LEED showed a ($3\sqrt{2} \times \sqrt{2}$)R45° pattern as shown in Fig. 1d. The pattern is described by streaked $3\sqrt{2}$ spots and sharp c(2×2) spots. AES spectra showed a significant reduction (35%) in the Sn(430)/Pt(237) AES ratio after annealing. This is consistent with alloy formation at the surface and/or Sn diffusion into the bulk.

Fig. 4a shows a large-area STM image of this surface. The atomic layer-high terraces terminate exclusively with step edges oriented along the ⟨1 0 0⟩ direction. Dark channels running along the [1 0 0] and [0 1 0] azimuths are now observed in all of the terraces, as was already observed for some terraces at a lower annealing temperature of 750 K. Furthermore, these channels are now more regularly spaced, with a dominant separation of $3\sqrt{2}$ times the Pt(1 0 0) surface-lattice constant. This separation gives rise to the LEED spots. However, other channel separations of integer multiples of $\sqrt{2}$ are also quite abundant and this explains the streaks in the LEED pattern. We suggest that the $3\sqrt{2}$ width is the most thermodynamically stable structure and that wider regions represent kinetically trapped structures. It is possible that these other structures are only slightly less energetically favorable than one with a $3\sqrt{2}$ characteristic width, and thus a distribution of these structures with different widths may form in thermodynamic equilibrium.

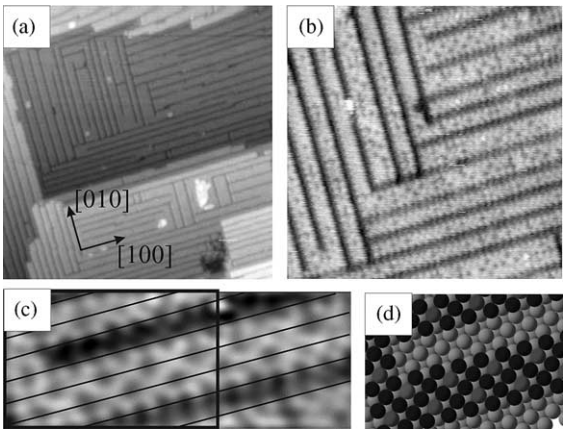

Fig. 4. STM images of a $3\sqrt{2}$ Sn/Pt(1 0 0) surface alloy. (a) Scan area (50 nm×50 nm). (b) Scan area (15 nm×15 nm). Flat terraces with channels along the ⟨1 0 0⟩ directions are observed. These channels have a predominant periodicity of $3\sqrt{2}$ times the surface-lattice constant of Pt(1 0 0), although wider separations are quite frequent. (c) Shows channels that are $4\sqrt{2}$ times the surface unit cell apart. Consequently the narrow terraces in between the channels is wider and the ordering of atomic-scale depressions in a p(2×2) pattern can be observed. These depressions are Sn-atoms alloyed in a Pt matrix. The lines drawn in (c) are equidistant with a separation of $\sqrt{2}$. From these lines it can be seen that three rows in between the narrow terraces are not imaged in STM. A ball model of the area marked by the rectangle is shown in (d). Black balls represent top-layer Pt-atoms and gray balls represent top-layer Sn-atoms. Light gray balls represent second-layer Sn or Pt atoms. There is no attempt made to discuss the structure of the second layer in this model because the STM images do not contain information about this layer. For a discussion of the second layer see Fig. 9.

Higher resolution STM images of the same surface are shown in Fig. 4b and c. These images show that the narrow terraces between the channels exhibit atomic scale dark depressions. In previous STM studies of Sn–Pt alloys it has been shown that a strong chemical contrast between Sn and Pt is observed with Sn always being imaged as depressions [9,12,28]. Therefore, the protrusions are Pt atoms and depressions correspond to alloyed Sn atoms within the same plane. The depressions, i.e., alloyed Sn atoms, often order locally into a p(2×2) structure on terraces that are wide enough to show this structure. The Sn atoms in this p(2×2) structure are mostly entirely within the terrace, i.e., the edges always appear bright and thus the terrace edges are Pt-terminated. However, this local ordering is frequently interrupted along these terraces by areas with higher Pt concentrations. The narrowest, but most abundant, terraces appear to be only three rows wide, i.e., $\sqrt{2}$ times the surface-lattice constant of Pt(1 0 0). The center row of these terraces often exhibits alternating dark depressions and bright protrusions that are due to alternating Sn and Pt atoms. The outside rows mainly consist of bright protrusions that are due to Pt atoms.

While the narrow terraces exhibit a distribution of widths, the channels separating these terraces are uniform in width. Tip-effects in STM often underestimate the width of narrow trenches. We can however use the atomic spacing given by the p(2×2) superstructure on the terraces to measure accurately the separation between the bright edge-rows of neighboring terraces. Equidistant lines drawn with separations of $\sqrt{2}$ times the surface-lattice constant of Pt(1 0 0) are superimposed on the STM image in Fig. 4c. This measurement illustrates that *three rows* in between the bright edge-rows of the terraces are not imaged in STM. There are two reasonable possibilities for these three "missing" rows. Either these rows are indeed missing, or there is only one missing row and the step edges of the narrow terraces are Sn-terminated. In the latter case, such step-edge Sn-atoms would be difficult to image because of the low contrast of Sn compared to Pt and therefore would give the impression of three missing rows. However, this is not the case and the structure of the "channels" between the terraces is discussed below in more detail with the help of ALISS spectra.

3.4. Sn/Pt(1 0 0) surface alloy annealed to 1000 K

Annealing of the surface to 1000 K causes any ordered superstructure in LEED to disappear and only a (1×1) pattern is observed (not shown). This surface is characterized by the STM image shown in Fig. 5. The surface is "flat", but consists of many small atomic layer-high islands. These islands still have step-edge orientations along the ⟨1 0 0⟩ azimuths, exhibit dark depressions along their center rows indicating the presence of Sn atoms, and also have preferred separation of $n\sqrt{2}$ times the surface-lattice constant of Pt(1 0 0). Therefore, this structure is very much reminiscent of that of the $3\sqrt{2}$ alloy. The main difference with that of the $3\sqrt{2}$ alloy is that a more isotropic surface is formed with predominantly square, compact islands instead of forming elongated terraces that gave rise to two domains with terraces aligned along the [1 0 0] and [0 1 0] directions, respectively. The formation of a surface with such an extremely high density of step edges after high temperature annealing is very unusual. Minimization of the free energy of the surface requires that

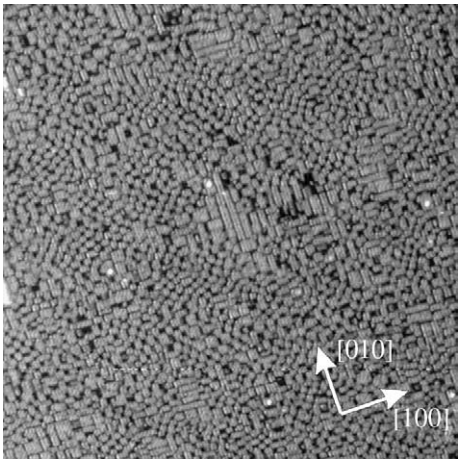

Fig. 5. Large scale (60 nm×60 nm) STM image of surface annealed to 1000 K. The surface is flat with a high density of small, often square islands. Some small areas remain that still exhibit $3\sqrt{2}$ ordering.

the energy cost for forming these step edges is balanced by reducing some other energy component. This energy component could be the reduction of strain in the surface layer. Furthermore, the entropy term in free energy contributes to a reduction of the total free energy by configurational disorder at elevated temperatures.

4. Discussion

Deposition of Sn on Pt(1 0 0) and subsequent annealing results in a series of metastable surface structures. For a complete interpretation of these structures the previously published angle-resolved low-energy alkali-ion scattering results need to be taken into account. To facilitate this discussion, these results are displayed in Fig. 6. Experimental details of these studies can be found in Ref. [15]. For each surface structure, polar scans along the [1 0 0] and [1 1 0] azimuths were taken and the intensity of ions scattered from both Pt and Sn target atoms were recorded. The critical angle for the onset of enhanced scattering at low polar angles contains information on the next-neighbor separation along the two azimuths investigated. The strongest variation is observed for scattering from Sn atoms with ions incident along the [1 1 0]

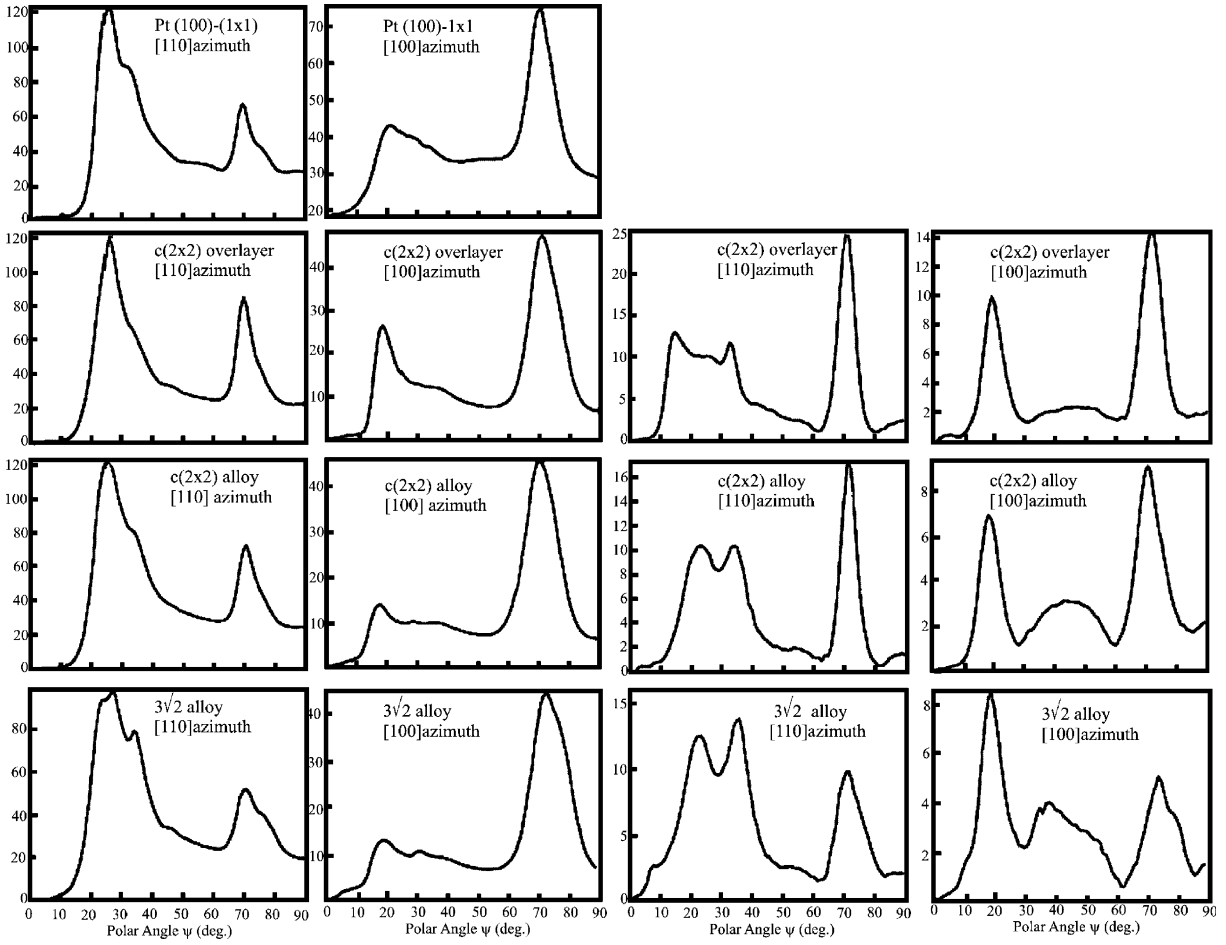

Fig. 6. Polar scans of alkali low-energy ion scattering spectra for different Sn/Pt(1 0 0) alloy structures along the [1 1 0] and [1 0 0] azimuths for ions scattered from Pt and Sn target atoms. These spectra are redisplayed from Ref. [15].

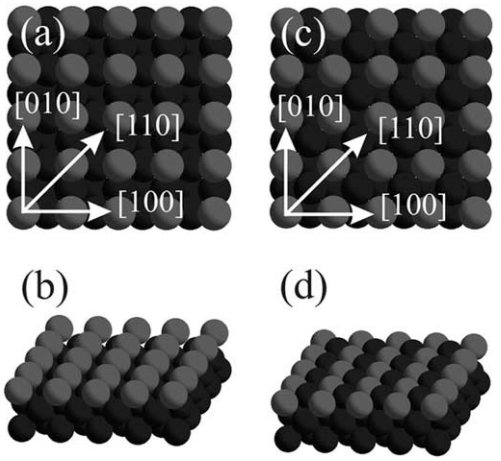

Fig. 7. Ball models for (a) and (b) c(2×2)-Sn *overlayer*, and (c) and (d) c(2×2)-Sn/Pt(1 0 0) *alloy*.

azimuth. In these scans, the critical angle shifts from 12° to 20° when the sample is annealed to 600 K. This is the hallmark for a transition from a c(2×2) *overlayer to an alloy*, because the Sn next-neighbor separation along the [1 1 0] azimuth for a c(2×2)-Sn overlayer is twice that for a c(2×2)-Sn/Pt(1 0 0) alloy. Ball models of these two surface structures are shown in Fig. 7. The critical angle for Sn scattering is unaltered along the [1 0 0] azimuth because the neighbor separations for a c(2×2) overlayer and c(2×2) alloy are identical along this azimuth. Interestingly, all of the Sn scans show a strong peak at 70°. This peak arises from the presence of Sn within the second layer, and this is direct evidence of alloy formation in the second layer. This establishes the correctness of the above-mentioned proposal that Pt which is expelled by lifting the hex-reconstruction alloys spontaneously at room temperature with deposited Sn.

Another open question that could not be unambiguously resolved by the STM studies alone was the issue of the termination of the narrow terraces of the $3\sqrt{2}$ alloy. If the step edges were terminated by Sn atoms as illustrated in Fig. 8a, then a local structure within the channels that resembled a c(2×2) overlayer structure would exist. This would cause a similar critical angle for Sn scattering as was observed for the Sn overlayer. In

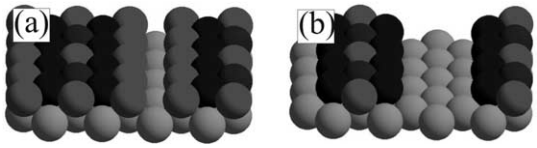

Fig. 8. Ball models for two possible terrace structures of the $3\sqrt{2}$ Sn/Pt(1 0 0) surface alloy. Light gray balls represent second-layer atoms. Black balls represent Pt-atoms and gray atoms represent Sn-atoms. In (a), the step edges terminate with Sn-atoms and only one row of atoms are missing in the surface layer per unit cell. In the model in (b) the step edges are Pt-terminated and three atomic rows are missing per unit cell. No attempt has been made to discuss the structure of the second layer in these models.

particular, a peak near 12° would be observed for a polar scan along the [1 1 0] azimuth. This was not the case. The main peak remains at the same position as was measured for the c(2×2) alloy. Therefore, we conclude that the step edges of the $3\sqrt{2}$ alloy are predominantly Pt-terminated and the dark channels consist of three missing rows as shown in Fig. 8b. Such an interpretation implies periodic Pt step-edges separated by $2\sqrt{2}$ along the [1 0 0] azimuth. This long, periodic separation of Pt next neighbors should result in a shift of the critical angle for Pt scattering along the [1 0 0] azimuth to very low angles. Indeed, a shoulder in the Pt scattering scan at ~4° can be observed for the $3\sqrt{2}$ alloy. The weakness of the signal can be partly explained by the fact that the ion flux per unit area at the surface decreases with the sine of the incidence angle and thus the scattering signal is expected to be small at extreme glancing angles. The separation between the Pt step-edge atoms is four times the surface-lattice constant of Pt(1 0 0) along the [1 1 0] azimuth, and this distance may be too large to result in a sufficiently enhanced Pt-scattering peak at low angles to be observed. For scattering from Sn atoms, low-angle peaks or shoulders are observed in scans along the [1 0 0] and [1 1 0] azimuths that are not observed in scans from the c(2×2) alloy surface. Along the [1 1 0] azimuth, a shoulder indicating a critical angle of ~7° can be discerned that indicates a next-neighbor separation that is longer than twice the surface-lattice constant. Such a long separation can only be present within the channels of missing

rows. Some randomly distributed, Sn adatoms adsorbed at the Pt-terminated step-edges could account for this peak. Such adatoms would have a distance of three times the lattice constant to the opposite step edge if measured along the [1 1 0] azimuth. These Sn adatoms could also cause the peak (shoulder) in Sn-scattering along the [1 0 0] azimuth at ~10°. Thus, in conclusion, the narrow terraces mostly consist of three atomic rows, with the center row often exhibiting alternating Sn and Pt atoms. The outer rows are Pt. Sn adatoms are randomly adsorbed along these Pt step-edges.

Small variations between the critical angles and peak positions in ALISS for Sn and Pt scattering for the same atomic constellations were discussed previously and assigned to relaxations of the surface atoms and in particular to outward buckling of Sn atoms from the surface alloy layer [14]. Additional features that were observed in ALISS spectra from the $3\sqrt{2}$ alloy that were not observed for the other structures included a double peak at small polar angles for Pt scattering along the [1 1 0] azimuth. We speculate that Pt atoms at the step edges of the narrow terraces either relax within the terrace plane or normal to the surface plane. Such relaxations change interatomic distances and angles, and would change the critical angle for Pt scattering. It is likely that two kinds of Pt atoms are present at the $3\sqrt{2}$ alloy surface, those Pt atoms at step edges and Pt atoms in the center of the terraces. The two Pt positions could give rise to the observed splitting of the low polar angle peak in Pt scattering along the [1 1 0] azimuth.

Combining the data from ALISS and STM studies allows us to propose a model for the narrow-terrace structure, however, the structure in between these terraces is less well characterized. Strong c(2×2) LEED spots, in the absence of a clear c(2×2) ordering of the narrow terraces, suggest a c(2×2) ordering of the second layer. Assuming that Sn preferably arranges in a c(2×2) constellation within the second layer, i.e., forming alternating Sn and Pt rows along the [1 0 0] direction, then two possibilities emerge for the location of Sn within the channels. Either there is one Sn row in the center of the channel or two Sn rows on either side of the channel. These two scenarios are illustrated by the regions on the left-hand and right-hand sides, respectively, of the ball models shown in Fig. 9a. On the left-hand side, the Sn atoms in the channel are entirely ''exposed'', while on the right-hand side, the number of Sn–Pt bonds is increased. Depending on the model, a Sn concentration at the surface of 42% or 25% can be obtained. These numbers were computed for a $(3\sqrt{2} \times 2\sqrt{2})$R45° unit cell, as shown in Fig. 9b, i.e., a unit cell that takes alternating Sn and Pt atoms in the center row of the narrow terraces into account. Previously, He-ISS studies and titration of the Pt sites with CO indicated that the surface Sn concentration does not significantly decrease when converting from a c(2×2) alloy to the $3\sqrt{2}$ alloy. This finding favors the constellation with the higher concentration of surface Sn. Sn alloyed within the channels can also explain an enhanced Sn-scattering peak at ~35° observed in ALISS spectra along the [1 0 0] azimuth. This peak is only dominant for the $3\sqrt{2}$ alloy and may arise from shadow cones formed by step-edge atoms and scattering from atoms on the lower terrace within the channels. This scattering geometry is schematically illustrated in Fig. 9c.

STM and AES results for the Sn/Pt(1 0 0) surface alloys can be compared to similar studies performed on a bulk Pt_3Sn(1 0 0) single-crystal sample [9]. The sample preparation procedure for those experiments involved sputtering and then annealing to successively higher temperatures to collect structural information at several temperatures. Because Sn is preferentially sputtered, the surface layer is initially depleted of Sn. Annealing the sample allows the surface layer to be replenished and eventually a surface layer with the bulk stoichiometry, i.e., a c(2×2) alloy layer, is reformed. During this process a variety of metastable structures, including a micro-facetted surface and a 'beaded-row' structure, were observed. Although there are obvious differences between surfaces of a bulk alloy and the surface alloys formed in our study, there are also interesting similarities and it is worthwhile to compare these two surfaces. For the bulk alloy surface, a c(2×2) structure is the thermodynamically stable surface termination. In the case discussed herein, the c(2×2) surface alloy is at best metastable. There are two main reasons why the c(2×2) surface alloy on Pt(1 0 0) is

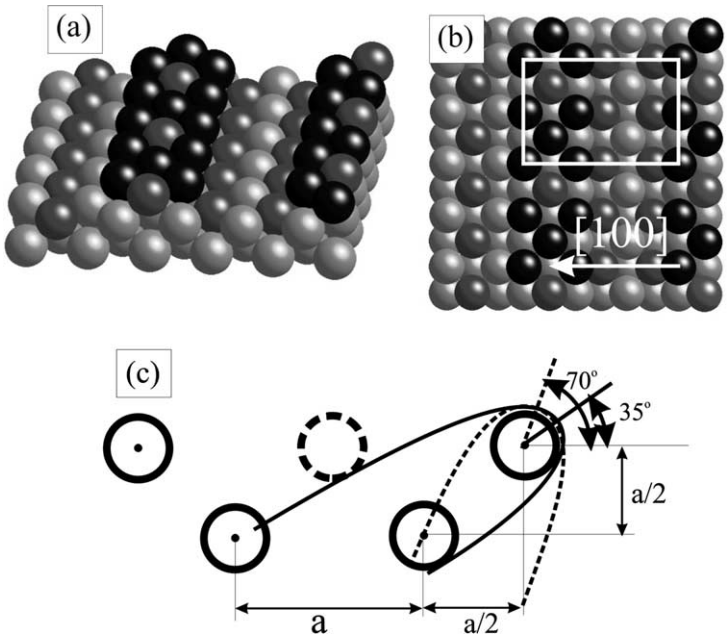

Fig. 9. Ball models for top and second layer atom arrangements. Black balls represent Pt-atoms in the top layer, light gray balls represent Pt-atoms in the second and consecutive layers, and gray balls represent Sn atoms in the top and second-layer. Two arrangements of Sn atoms in the second layer are considered. On the left side of (a) and (b) the Sn atoms are in the center of the three missing rows, on the right side the Sn atoms are situated on the left and right of the three missing rows. In (b) a $(3\sqrt{2} \times 2\sqrt{2})$R45° unit cell is drawn in. This unit cell contains 42% Sn at the surface. The shadow cones for an ALISS experiment with incidence along the [1 0 0] azimuth are schematically illustrated in (c). At a polar angle of 70° increased scattering from the second layer atoms are observed. If a top-layer row is missing (indicated by the dashed circle) an additional increased scattering peak can be observed at a polar angle of ~35°.

not stable: (i) the pure-Pt substrate has a smaller lattice constant than the $Pt_3Sn(1\,0\,0)$ alloy substrate. This results in additional compressive strain in the case of the surface alloy as a consequence of the lattice mismatch between the surface layer and the substrate; and (ii) the greater concentration gradient of Sn between the surface and the bulk more strongly drives diffusion of Sn into the bulk for the case of the surface alloy. The opposite is happening in the case of a Sn-depleted surface layer of a bulk alloy crystal.

One of the metastable structures observed on the $Pt_3Sn(1\,0\,0)$ alloy surface was the so-called "beaded-row" structure (see Fig. 5b in Ref. [9]). This structure, although not discussed in detail in Ref. [9], appears to show some resemblance to the $3\sqrt{2}$ structure discussed in this communication. It also consists of three atomic rows with dark depressions, most likely alloyed Sn atoms, at the center row. The width of these "channels" is only one atomic row, however, in contrast to the triple atomic-row separation observed for the surface alloy. Such formation of missing rows or channels at the surface is likely to be driven by strain. Alloying of larger atoms into the surface layer, or segregation of Sn from the bulk to the surface on a Sn-depleted surface layer, induces compressive strain that can be relaxed at the step edges of missing-row structures. The largest strain is along the most densely packed, $\langle 1\,1\,0\rangle$, direction. Forming missing rows along the $\langle 1\,0\,0\rangle$ direction allows strain to be relieved in both the [1 1 0] and [−1 1 0] directions at the same time. However, any residual strain along the $\langle 1\,0\,0\rangle$ direction cannot be relieved by the formation of these channels. This may be the reason why the $3\sqrt{2}$ alloy structure fragments into

smaller, square islands (with some tendency to form a checkerboard-like structure) at higher temperatures.

This newly gained insight into the surface alloy structure can now be applied to develop a better understanding of structure–chemistry relationships of Sn–Pt alloys. Chemisorption studies on Sn/Pt(1 0 0) surfaces have been carried out using CO [17], NO [18], and C_2D_2 [19,20]. Those studies established that it matters greatly whether Sn is present at the surface in an adlayer or incorporated into the surface plane to form an alloy. The c(2×2)-Sn overlayer eliminated all chemisorption at the surface, while alloyed Sn only partially inhibited chemisorption and reaction. Alloyed Sn effectively blocked some chemisorption, and the saturation coverage was diminished significantly on the alloys compared to that on the clean Pt(1 0 0) surface. A coverage of 0.77-ML CO can be chemisorbed on Pt(1 0 0), but this is reduced to 0.28 ML on the c(2×2) alloy and further to 0.25 ML on the $3\sqrt{2}$ alloy at 150 K. A model was proposed with CO adsorbed in a p(2×2) arrangement on surface Pt atoms yielding a theoretical coverage in the monolayer of 0.25-ML CO.

Saturation monolayer coverages of NO chemisorbed on Sn/Pt(1 0 0) surfaces follow the same trend as those for CO. The NO coverage was reduced from 0.73 ML on the Pt(1 0 0) surface to 0.33 and 0.22 ML on the c(2×2) and $3\sqrt{2}$ alloys, respectively. On the Pt(1 0 0) surface, NO adsorbed nearly reversibly, with some decomposition yielding N_2 and O_2 desorption products in TPD. However, N_2O production was observed during TPD from both alloys, with more N_2O desorbing from the c(2×2) alloy. This decomposition pathway was proposed to occur due to the formation of a dinitrosyl species which formed N_2O upon heating. The formation of p(2×2) alloy structures and pure-Pt "patches" on the terraces of the $3\sqrt{2}$ alloy may explain the decrease in N_2O yield on this surface compared to that on the c(2×2) alloy.

The most interesting changes in chemistry were observed in chemisorption studies of C_2D_2 on the Sn/Pt(1 0 0) surfaces. The saturation coverage of 0.5-ML C_2D_2 on the Pt(1 0 0) surface was reduced to 0.32 and 0.25 ML on the c(2×2) and $3\sqrt{2}$ alloys, respectively. The greater reduction in chemisorption capacity on the $3\sqrt{2}$ alloy may indicate that C_2D_2 does not adsorb within the channels of this structure. However, on the $3\sqrt{2}$ alloy only, benzene production was observed during TPD. *This result is significant because it was thought previously that acetylene cyclotrimerization required threefold metallic sites to occur. Based on our STM images and the resulting model of the* $3\sqrt{2}$ *surface, no hexagonal Pt sites are present on this surface prior to acetylene adsorption*. The regions between Pt missing rows exhibit predominately p(2×2)-Sn ordering and adjacent Pt atoms form chains along the ⟨1 1 0⟩ direction. Furthermore, due to imperfect ordering in these p(2×2) regions, pure-Pt fourfold-hollow sites exist on the $3\sqrt{2}$ alloy. These fourfold Pt sites are not expected to be active for cyclotrimerization because the reaction does not occur on clean Pt(1 0 0). In our structural model for the $3\sqrt{2}$ alloy structure we propose that the step edges next to the channels are pure Pt. Thus, depending on the composition of the second layer there may also exist twofold Pt-bridge sites at the step edges. Therefore, we propose that twofold Pt-bridge sites, either on the (1 0 0) plane or at ⟨1 0 0⟩ step edges, can promote this reaction. This reaction was previously observed to occur to a small extent on both the (2×2) and $(\sqrt{3}\times\sqrt{3})$R30°-Sn/Pt(1 1 1) surface alloys where threefold and twofold, pure-Pt bridging sites are present, respectively.

5. Conclusions

Deposition of Sn on the Pt(1 0 0) surface and subsequent annealing results in a series of metastable surface structures, as probed herein by STM. A c(2×2)-Sn adlayer structure can be formed, but with concomitant surface alloying. A c(2×2) alloy which has Sn and Pt atoms arranged in a "checkerboard" fashion with Pt atoms surrounded only by Sn, and vice versa, that has been studied in the past regarding its chemisorption properties is at best a metastable structure that always incorporates a mixture of other phases. The most intriguing alloy structure is the $(3\sqrt{2}\times\sqrt{2})$R45° surface alloy, which retains a similar surface Sn-atom concentration as the c(2×2) alloy, but forms reactive, pure-Pt twofold

bridge sites (surprisingly) via redistribution of Sn and a ''missing-row'' type of reconstruction. This alloy is an ''open'' surface structure with a high density of narrow terraces and consequently a high density of step edges. Minimization of the stress introduced by substitutional incorporation of the larger Sn atoms into the Pt substrate lattice may be responsible for the high step-edge concentration. These step edges appear to preferentially terminate with Pt. Sn is alloyed in between the narrow terraces and on top of the terraces in a fashion that maximizes the number of Sn–Pt bonds. We suggest that the twofold, pure-Pt bridge sites at the Pt-terminated step edges or on top of the terraces play an important role in explaining the chemistry of this surface. In particular, it appears that cyclotrimerization of acetylene to benzene, only observed on the $(3\sqrt{2} \times \sqrt{2})$R45° surface alloy and not on Pt(1 0 0) nor the c(2×2) alloy, is correlated to the presence of pure-Pt twofold bridge sites. Thus, this reaction does not require threefold metallic sites to occur. Higher temperature annealing can form alloy surfaces with extremely high densities of step edges, but the chemistry of such Pt–Sn surfaces has not yet been investigated.

Acknowledgements

This material is based upon work supported by the National Science Foundation under Grant No. 0213583.

References

[1] G. Ritz, M. Schmid, P. Varga, A. Borg, M. Rønning, Phys. Rev. B 56 (1997) 10518.
[2] Y.Y. Yeo, C.E. Wartnaby, D.A. King, Science 268 (1995) 1731.
[3] W. Hebenstreit, G. Ritz, M. Schmid, A. Biedermann, P. Varga, Surf. Sci. 388 (1997) 150.
[4] Y. Gauthier, P. Dolle, R. Baudoing-Savois, W. Hebenstreit, E. Platzgummer, M. Schmid, P. Varga, Surf. Sci. 396 (1998) 137.
[5] M. Schmid, W. Hofer, P. Varga, P. Stoltze, K.W. Jacobsen, J.K. Nørskov, Phys. Rev. B 51 (1995) 10937.
[6] J. Cathro, J. Electrochem. Soc. 116 (1986) 1608.
[7] F. Dautzenberg, J. Melle, P. Biloen, W. Sachtler, J. Catal. 63 (1980) 119.
[8] S. Speller, U. Bardi, in: D.P. Woodruff (Ed.), Surface Alloys and Alloy Surfaces, The Chemical Physics of Solid Surfaces, vol. 10, Elsevier, Amsterdam, 2002 (Chapter 6).
[9] M. Hoheisel, J. Kuntze, S. Speller, A. Postnikov, W. Heiland, I. Spolveri, U. Bardi, Phys. Rev. B 60 (1999) 2033.
[10] A.N. Haner, P.N. Ross, U. Bardi, Surf. Sci. 249 (1991) 15.
[11] W.C.A.N. Ceelen, A.W. Denier van der Gon, M.A. Reijme, H.H. Brongersma, I. Spolveri, A. Atrei, U. Bardi, Surf. Sci. 406 (1998) 264.
[12] J. Kuntze, S. Speller, W. Heiland, A. Atrei, I. Spolveri, U. Bardi, Phys. Rev. B 58 (1998) 16005.
[13] M.T. Paffett, R.G. Windham, Surf. Sci. 208 (1989) 34.
[14] Y.D. Li, M.R. Voss, N. Swami, Y.L. Tsai, B.E. Koel, Phys. Rev. B 56 (1997) 15982.
[15] Y. Li, B.E. Koel, Surf. Sci. 330 (1995) 193.
[16] M.T. Paffet, A.D. Logan, R.J. Simonson, B.E. Koel, Surf. Sci. 250 (1991) 123.
[17] C. Panja, B.E. Koel, Isr. J. Chem. 38 (1998) 365.
[18] C. Panja, B.E. Koel, J. Phys. Chem. A 104 (2000) 2486.
[19] C. Panja, N.A. Saliba, B.E. Koel, Catal. Lett. 68 (2000) 175.
[20] C. Panja, N.A. Saliba, B.E. Koel, J. Phys. Chem. B 105 (2001) 3786.
[21] D.E. Beck, M. Batzill, C. Baur, J. Kim, B.E. Koel, Rev. Sci. Inst. 73 (2002) 1267.
[22] P. Heilmann, K. Heinz, K. Müller, Surf. Sci. 83 (1979) 487.
[23] J.J. McCarroll, Surf. Sci. 53 (1975) 297.
[24] A. Borg, A.-M. Hilmen, E. Bergene, Surf. Sci. 306 (1994) 10.
[25] C. Berg, H.J. Venvik, F. Strisland, A. Samstad, A. Borg, Surf. Sci. 409 (1998) 1.
[26] H.J. Venvik, C. Berg, A. Borg, S. Raaen, Phys. Rev. B 53 (1996) 16587.
[27] M. Batzill, B.E. Koel, Surf. Sci. 498 (2002) L85.
[28] M. Batzill, D.E. Beck, B.E. Koel, Surf. Sci. 466 (2000) L821.